ASME Journal of Biomechanical Engineering
Online journal at:
https://asmedigitalcollection.asme.org/biomechanical

Quantification of Cartilage Poroelastic Material Properties Via Analysis of Loading-Induced Cell Death

Alexander Kotelsky
Department of Biomedical Engineering,
University of Rochester,
Rochester, NY 14627

Joseph S. Carrier
Department of Biomedical Engineering,
University of Rochester,
Rochester, NY 14627

Mark R. Buckley[1]
Department of Biomedical Engineering,
University of Rochester,
Rochester, NY 14627
e-mail: mark.buckley@rochester.edu

Articular cartilage (AC) is a load-bearing tissue that covers long bones in synovial joints. The biphasic/poroelastic mechanical properties of AC help it to protect joints by distributing loads, absorbing impact forces, and reducing friction. Unfortunately, alterations in these mechanical properties adversely impact cartilage function and precede joint degeneration in the form of osteoarthritis (OA). Thus, understanding what factors regulate the poroelastic mechanical properties of cartilage is of great scientific and clinical interest. Transgenic mouse models provide a valuable platform to delineate how specific genes contribute to cartilage mechanical properties. However, the poroelastic mechanical properties of murine articular cartilage are challenging to measure due to its small size (thickness ~ 50 microns). In the current study, our objective was to test whether the poroelastic mechanical properties of murine articular cartilage can be determined based solely on time-dependent cell death measurements under constant loading conditions. We hypothesized that in murine articular cartilage subjected to constant, sub-impact loading from an incongruent surface, cell death area and tissue strain are closely correlated. We further hypothesized that the relationship between cell death area and tissue strain can be used—in combination with inverse finite element modeling—to compute poroelastic mechanical properties. To test these hypotheses, murine cartilage-on-bone explants from different anatomical locations were subjected to constant loading conditions by an incongruent surface in a custom device. Cell death area increased over time and scaled linearly with strain, which rose in magnitude over time due to poroelastic creep. Thus, we were able to infer tissue strain from cell death area measurements. Moreover, using tissue strain values inferred from cell death area measurements, we applied an inverse finite element modeling procedure to compute poroelastic material properties and acquired data consistent with previous studies. Collectively, our findings demonstrate in the key role poroelastic creep plays in mediating cell survival in mechanically loaded cartilage and verify that cell death area can be used as a surrogate measure of tissue strain that enables determination of murine cartilage mechanical properties. [DOI: 10.1115/1.4065194]

Introduction

Articular cartilage is a load-bearing tissue that covers and protects the ends of long bones and enables painless and nearly frictionless movement of synovial joints [1]. The functionality of AC is endowed by its unique and intricate structure, composition, and mechanical properties. Specifically, cartilage possesses a water-saturated, collagen-rich extracellular matrix (ECM) interspersed with negatively charged proteoglycans that help provide the tissue with a high swelling pressure and a high resistance to compression [2]. Due to the presence of both a solid component (the ECM) and a fluid component (water), cartilage can be modeled as a biphasic/poroelastic material whose mechanical response is determined by the properties and interactions between these two phases [3]. For instance, when cartilage is compressed by a constant load, interstitial water—an incompressible material—provides fluid load support that helps resist the applied force [4]. However, over time, water is slowly squeezed from very small pores in the ECM and the tissue progressively deforms at a rate proportional to its permeability (k, a measure of how easily fluid flows in or out) to an equilibrium deformation proportional to the solid matrix Young's modulus (E, a measure of intrinsic stiffness).

Because cartilage protects joints by distributing loads [5], absorbing impact forces [6,7], and reducing friction [8–11], alterations in cartilage poroelastic mechanical properties are thought to have an adverse effect on joint health and have been shown to precede joint degeneration in the form of osteoarthritis [12,13]. However, what molecular constituents govern the poroelastic mechanical properties of articular cartilage is incompletely understood. A promising avenue to identify specific structural components responsible for regulating cartilage poroelastic mechanical properties is through the use of transgenic mouse

[1]Corresponding author.

Manuscript received May 16, 2023; final manuscript received March 20, 2024; published online April 8, 2024. Assoc. Editor: David M. Pierce.

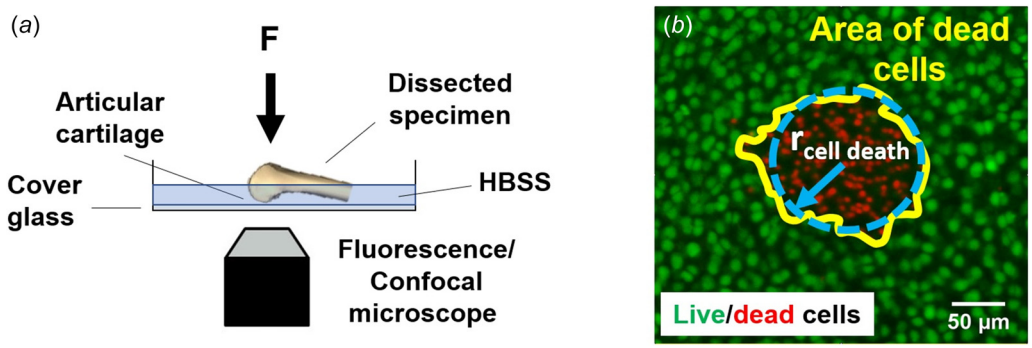

Fig. 1 Induction and quantification of cell death. (*a*) Schematic representation of the mechanical testing device. Dissected specimens (femurs or humeri) were placed on the cover glass of the testing device and compressed statically with a prescribed subimpact load (*F*) and loading duration, or dynamically with a frequency of 0.1 Hz. Cartilage on the articular surface of the distal femoral condyles or the humeral head was visualized before and after the application of *F* using a fluorescence or confocal microscope. (*b*) Representative micrograph of the articular surface on the lateral condyle of a murine distal femur subjected to *F* = 0.5 N of static loading. The area of cell death is the area outlined by the yellow contour, defined as the contour within which cells lost calcein fluorescence (green) and gained PI fluorescence (red). The radius of the area of cell death ($r_{\text{cell death}}$) was quantified assuming the area was a perfect circle. (Color version online.)

models. Nevertheless, assessing poroelastic mechanical properties in mouse cartilage is difficult due to its very small size. Thus, to our knowledge, only a few research groups have quantified these properties in mice using nano- and micro-indentation techniques [14–16].

An alternative approach to determine mouse cartilage poroelastic mechanical properties may be through assessment of time-dependent cell death. This approach is motivated by previous studies demonstrating that in axially loaded bovine cartilage explants, the extent of cell death increases with load duration [17]. Since tissue strain also increases with load duration in poroelastic materials [3], these findings suggest that there may be a consistent relationship between chondrocyte death and tissue strain. Thus, in cartilage specimens subjected to a (known) constant load, it may be feasible to quantify strain over time based on the time evolution of cell death area. From the applied load and time-dependent strain, tissue poroelastic material properties may then be determined using inverse methods.

Importantly, in previous studies, we described an experimental platform enabling assessment of the extent of cell death (cell death area) in murine cartilage-on-femur and cartilage-on-humerus explants subjected to a constant load from an incongruent surface [18–20]. In the current study, our objective was to test whether time-varying cell death measurements acquired using this platform can be used (in combination with inverse finite element modeling) to assess murine cartilage poroelastic mechanical properties. We hypothesized that cell death area and tissue strain are strongly correlated in this platform, and that the specific relationship between these parameters can be used to determine tissue permeability and solid matrix Young's modulus from measurements of time-dependent cell death area.

Methods

Study Design. Collectively, 91 murine cartilage-on-bone explants (52 distal femurs and 39 humeri) obtained from 8 to 10 weeks old female BALB/c mice were tested in this study. Only female mice were used in order to maintain uniformity in specimen size and geometry. A total of 34 femurs and 21 humeri were randomly assigned to one of six loading duration groups (1 N applied for 5 s, 10 s, 30 s, 60 s, 300 s, or 900 s, $n = 5$–6 femurs per group, 3–6 humeri per group) to investigate the effects of loading duration on cell vulnerability and establish poroelastic creep curves. Humeri were not assigned to the 900 s group because they reached poroelastic equilibrium earlier (at 60 s). Additionally, 18 femurs and 18 humeri were randomly assigned to one of three loading groups (0.1 N, 0.5 N, or 1 N applied for 5 min, $n = 6$ specimens per group) to establish the relationship between peak tissue deformation and cell death area. Finally, five of the distal femurs were used to establish that cell death area measurements—in combination with inverse FE modeling and the relationship between cell death area and tissue deformation—can be used to determine tissue poroelastic material properties.

Specimen Preparation. Experiments were approved by the University of Rochester Committee on Animal Resources (UCAR-2013-017). Humeri and distal femurs with fully intact articular cartilage were carefully dissected from the glenohumeral and tibiofemoral joints of 8–10 weeks old female BALB/c mice immediately after sacrifice using a previously established technique [19]. Briefly, surrounding soft tissue was carefully removed, leaving intact cartilage-on-bone complexes. Femurs were cut 8 mm above the tibiofemoral joint, while humeri were kept fully intact. Dissected specimens were hydrated in Hank's Balanced Salt Solution (HBSS) at a physiological *p*H (7.4±0.02) and in an iso-osmotic environment (303±1 mOsm) throughout all experiments, which were performed at room temperature.

Assessing the Effects of Loading Duration on Mechanically-Induced Chondrocyte Death. The spatial extent of cell injury/death resulting from mechanical loading was quantified using a previously established microscope-mounted in vitro mechanical testing device [19]. Briefly, dissected specimens were vitally stained at 37 °C for 30 min with 10 μM calcein AM (Life Technologies, Eugene, OR), an indicator of viable cells with intact membranes, and then washed in HBSS for at least 10 min to remove excess extracellular dye prior to mechanical testing. Vitally stained specimens were then placed on top of the cover glass of the mechanical testing device, just above the objective of an inverted microscope such that the articular surfaces on the femoral condyles or the humeral heads were in contact with the glass and visible through the microscope objective (Fig. 1(*a*)). To stabilize humeral specimens on the testing device, a wooden applicator was fixed to the distal side of the bone using cyanoacrylate glue. Using a cylindrical weight, a subimpact load (*F*) of 1 N was applied on top of the patellofemoral grove of the dissected femurs ($n = 5$–6/loading group), or on top of the greater tuberosity of the humeri ($n = 4$–6/loading group except for the 5 s loading group where $n = 3$) for 0, 5, 10, 30, 60, 300, or 900 s in order to determine the effect of subimpact loading duration on cell vulnerability (Fig. 1(*a*)). The load was imposed by manually lowering the cylindrical weight through a smooth guide block, and a calibrated strain gauge was used to

measure the applied load over time. Application of load compressed the layer of cartilage lining the femoral condyles or the humeral head. Note that the 900 s humerus group was omitted from the study because the transient size of the area of cell injury/death reached equilibrium at 60 s (see Results). Since the instantaneous magnitude of the reaction force did not substantially exceed the force observed at equilibrium (due to negligible kinetic energy at impact), the application of a sustained 1 N load was termed "sub-impact" (Fig. S1 available in the Supplemental Materials on the ASME Digital Collection). Thus, the magnitude of the applied load was computed as mg, where m is the mass of the cylindrical impactor and g is the acceleration due to the gravity.

To quantify the spatial extent of cell death due to the applied mechanical loading regimen, the articular surfaces of the femoral condyles or humeral head were imaged under fluorescence illumination with a 4X dry lens (NA = 0.13) on an inverted epifluorescence microscope (Olympus IX-81) at baseline (i.e., before the application of mechanical load) and 5 min after mechanical load was removed (Fig. 1(*b*)). Additionally, after post-load imaging, select specimens ($n = 5$) were stained with 40 μg/mL propidium iodide (PI, Life Technologies, Eugene, OR), an indicator of cells with ruptured membranes, and re-imaged. Specimen loading was monitored in real-time, and only small amounts of rotation or sliding were observed. In particular, specimens typically slid less than a few microns.

The radius of the area of cell death ($r_{\text{cell death}}$)—i.e., the radius of the area encompassing cells that lost calcein (green) fluorescence—was manually quantified in ImageJ (Fig. 1(*b*)). To ensure that manual measurements of $r_{\text{cell death}}$ were repeatable, an inter-rater reliability analysis was performed. Specifically, a total of four blinded raters quantified $r_{\text{cell death}}$ in a subset of images ($n = 6$). The intraclass correlation coefficient—a measure of reliability that varies between 0 and 1—was calculated in Excel (Microsoft Corporation, Redmond, WA). The intraclass correlation coefficient was found to be 0.90, suggesting excellent reliability.

Establishing the Relationship Between Cartilage Strain and Radius of Cell Death. To establish the relationship between tissue strain and cell death on the articular surface, first, cartilage-on-bone specimens were subjected to a range of static loads (0.1 N, 0.5 N, or 1 N, $n = 6$/group) for 5 min. For each test, $r_{\text{cell death}}$ was quantified as described earlier. Since cell death predominantly occurred on lateral femoral condyles, only lateral condyles were used to establish the cell death/tissue strain relationship in femoral cartilage-on-bone specimens. Note that the higher levels of cell death observed on the lateral condyles are likely due to the way the sample is mounted and the smaller radius of curvature on the lateral side.

After assessment of $r_{\text{cell death}}$, specimens were stored at −20 °C for 1–2 weeks and subsequently used to quantify the peak tissue deformation induced by each prescribed load (0.1 N, 0.5 N, or 1 N, $n = 6$/group) using a previously established method [20]. Briefly, after thawing, specimens were fluorescently stained for 1 h at 23 °C with 10 μg/mL 5′-DTAF (Sigma-Aldrich, St. Louis, MO), a fluorescent dye that binds to amine groups in proteins and enables visualization of the cartilage ECM under fluorescent illumination. Specimens were then washed in HBSS for 3 h to wash out the excess dye and placed on the cover glass of the mechanical testing device (Fig. 1(*a*)). Cartilage on the lateral femoral condyles or humeral head was imaged both before and 5 min after application of the prescribed load magnitude using an Olympus FV1000 laser scanning confocal microscope with a 40X dry lens (LUCPLFLN, NA = 0.6) to obtain three-dimensional (3D) image stacks with a spatial resolution of 0.31 μm/pixel along z-axis (1.64 μm/slice) (Fig. 2). Note that in order to compensate for the refractive index mismatch between the immersion media on the objective lens (i.e., air) and the specimen-hydrating HBSS buffer, the z-axis of the acquired image stacks was scaled by 1.33 [21]. Using the acquired 3D confocal z-stacks (Fig. 2), the stretch ratio at the center of contact (λ_z) was defined as $\lambda_z = \text{Thickness}_{\text{compressed}}/\text{Thickness}_{\text{baseline}}$, where the cartilage thickness under compression ($\text{Thickness}_{\text{compressed}}$) and the baseline cartilage thickness ($\text{Thickness}_{\text{baseline}}$) were measured at the center of contact using a previously described MATLAB algorithm [20]. The Lagrangian strain at the center of contact (E_z) was computed according to $E_z = \frac{1}{2}\left(\lambda_z^2 - 1\right)$. After quantifying both tissue strain (E_z) and radius of the area of cell death ($r_{\text{cell death}}$) in each tested specimen for each prescribed load, the relationship between these parameters was determined through a linear regression analysis.

Characterization of Poroelastic Creep in Murine Articular Cartilage. While we have previously used confocal microscopy to characterize the equilibrium deformation of murine AC under different static loading conditions [20], due to the slow acquisition speed of confocal image stacks, it is more challenging to quantify *transient* deformation of murine AC during poroelastic creep. Therefore, we used the relationship between $r_{\text{cell death}}$ and loading duration in combination with the relationship between $r_{\text{cell death}}$ and E_z (see previous sections) to determine the relationship between E_z and loading duration (i.e., the poroelastic creep curve of murine AC). We first used our experimentally determined E_z versus $r_{\text{cell death}}$ curves to determine a linear equation that converts $r_{\text{cell death}}$ to E_z. Finally, we applied this conversion to transform our experimentally determined $r_{\text{cell death}}$ versus loading duration curves to E_z versus loading duration (poroelastic creep) curves. Note that specimens that did not exhibit cell injury/death in the loading duration study were not included in the characterization of poroelastic creep since E_z could not be quantified.

Characterization of the Poroelastic Material Properties of Murine Articular Cartilage Using Inverse Finite Element Analysis. To quantify poroelastic material properties, a finite element-based optimization approach was used in combination with poroelastic creep curves acquired as described earlier. First, five femur-on-bone specimens previously stained with DTAF and imaged in 3D to determine peak strain after force application were randomly selected. For each specimen, the geometry (thickness and curvature) of the cartilage on the lateral condyle was determined based on the acquired 3D image stacks (Fig. 2) and used to construct

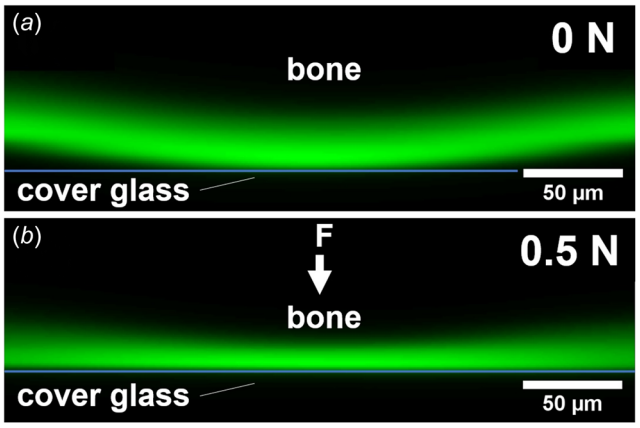

Fig. 2 Sagittal cross sections of articular cartilage before and during compressive loading. Representative sagittal cross sections from a confocal image stack of fluorescently labeled (green) articular cartilage on a murine lateral femoral condyle obtained (*a*) before and (*b*) after application of a static load of 0.5 N for 5 min. The top boundary is the cartilage–bone interface, while the horizontal line denotes the boundary of the cover glass. Acquired images were used to determine peak tissue compressive strains induced by force application in order to establish the relationship between tissue strain and radius of cell death. The baseline image (*a*) was also used to construct a finite element model from the measured thickness and radius of curvature (Fig. 3).

specimen-specific poroelastic/biphasic FE models loaded by a flat rigid surface (Fig. 3).

The model element size was determined based on a mesh convergence analysis. A full model was used instead of a partial model exploiting symmetry (e.g., a quarter model) since the forward simulation run time was reasonable (<30 min). The hydraulic permeability (k) of the cartilage was assumed to be independent of strain, and the solid matrix of the cartilage was assumed to be a neo-Hookean material described by a solid matrix Young's modulus (E) and drained Poisson's ratio (ν). To determine E for each specimen/model, a parameter optimization routine was implemented in FEBio to identify the value of E where the equilibrium Lagrangian strain at the center of contact (E_z) induced by a simulated load of 0.4 N (the force on the lateral condyle from the cover glass after application of a 1 N load on the distal femur, Fig. S2 available in the Supplemental Materials on the ASME Digital Collection) was equal to the experimentally measured equilibrium tissue strain (E_z). The parameter E_z was calculated according to $E_z = \frac{1}{2}\left(\lambda_z^2 - 1\right)$, where $\lambda_z = \text{Thickness}_{\text{compressed}}/\text{Thickness}_{\text{baseline}}$ with $\text{Thickness}_{\text{compressed}}$ and $\text{Thickness}_{\text{baseline}}$ both measured at the center of contact. Note that the equilibrium behavior of the model is insensitive to k. Next, to determine k for each specimen/model, E was assigned its measured value and the temporal evolution of tissue strain after application of an 0.4 N load was simulated across multiple iterations of k. The specimen-specific value of k was identified when the simulated and experimentally measured creep curves (i.e., curves representing the temporal evolution of E_z) induced by application of an 0.4 N load on the lateral condyle were optimally matched. In all models, the Poisson's ratio was taken to be 0.25 [20].

Statistical Analysis. The radius of the area of chondrocyte death ($r_{\text{cell death}}$) for each loading duration was compared to the control (0 s) group using a Kruskal–Wallis test with Dunnett's posthoc analysis ($\alpha = 0.05$). For both humeri and distal femurs, linear regression analysis was performed to correlate and determine the relationship between Lagrangian strain at the center of contact (E_z) and radius of the area of cell death ($r_{\text{cell death}}$). The linear relationship between E_z and $r_{\text{cell death}}$ (i.e., $E_z = m r_{\text{cell death}} + b$) was used to calculate E_z for each loading duration, and the standard deviation of E_z was computed using the error propagation formula $\sigma_{E_z} = \sqrt{m^2 r_{\text{cell death}}^2 \left[\left(\frac{\sigma_m}{m}\right)^2 + \left(\frac{\sigma_{r_{\text{cell death}}}}{r_{\text{cell death}}}\right)^2\right] + \sigma_b^2}$. All statistical analyses were conducted in GraphPad Prism (version 6.01, La Jolla, CA) or in Excel (Microsoft Corporation, Redmond, WA).

Results

The Effect of Sub-Impact Loading Duration on Mechanically-Induced Chondrocyte Death. Statistically significant chondrocyte death compared to control (0 s loading) was observed on the articular surfaces of femoral condyles and humeral heads when the tissue was

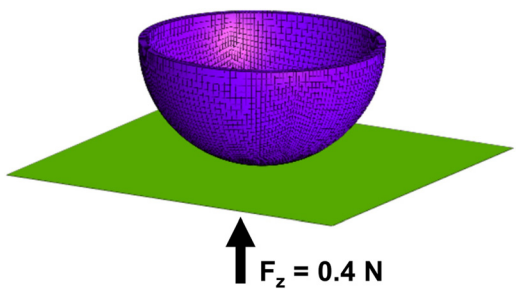

Fig. 3 Model geometry for inverse finite element analysis. 3D finite element model (FEM) used for inverse finite element analysis (FEA) to determine specimen-specific poroelastic tissue properties. A force F_z was applied via a rigid platen, and the strain (E_z) was tracked over time.

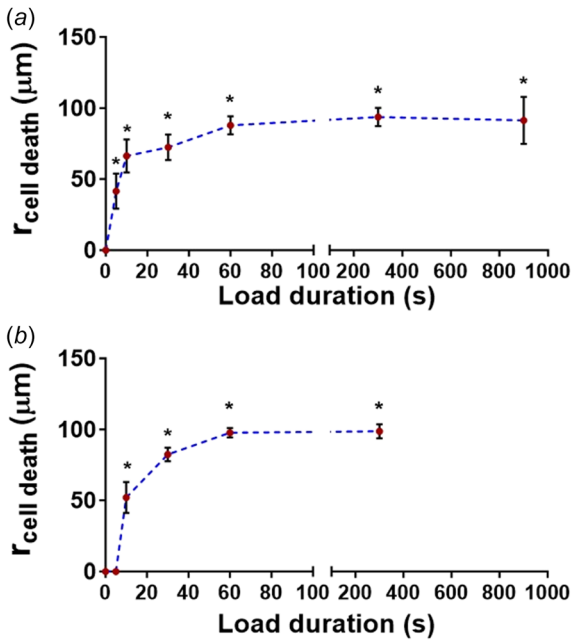

Fig. 4 Cell death as a function of loading duration. Temporal evolution of the radius of the area of cell death ($r_{\text{cell death}}$) when (*a*) femurs (both condyles) and (*b*) humeri were subjected to a 1 N static load applied for different durations. Data are mean ±SD. (*) denotes significant difference compared to cell death prior to application of load. The cell death profiles resemble a typical creep curve where $r_{\text{cell death}}$ gradually increases until equilibrium is reached.

subjected to a constant load for a prolonged duration (Fig. 4). In femoral condyles, cell death radius was higher than control for durations of 5, 10, 30, 60, 300, and 900 s. In humeral heads, loading for less than 10 s did not induce significant cell injury/death (Fig. 4),

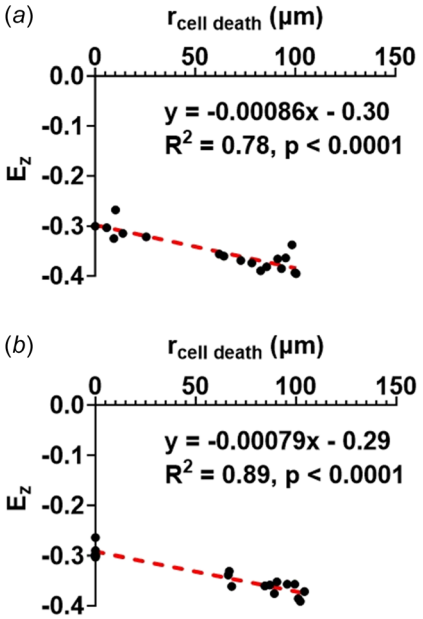

Fig. 5 Correlation between tissue strain and cell death. Lagrangian strain at the center of contact (E_z) on (*a*) femoral lateral condyles and (*b*) humeral heads versus radius of cell death ($r_{\text{cell death}}$) after 5 min static loading to 0.1 N, 0.5 N, and 1 N. Strong and significant correlations between E_z and $r_{\text{cell death}}$ were observed for both femurs and humeri. Each data point represents a single specimen subjected to a specific applied load. The dashed lines are curve fits obtained from linear regression analyses.

but cell death radius was higher than control for durations of 10, 30, 60, 300, and 900 s. In both femurs and humeri, a constant sub-impact load of 1 N induced a gradual increase in the radius of dead cells until the spatial extent of cell death reached equilibrium and stayed constant regardless of the loading duration.

Relationship Between Cartilage Strain and Radius of Cell Death. Lagrangian strain at the center of contact (E_z) was strongly correlated with radius of cell death ($r_{\text{cell death}}$) for both femoral lateral condyles ($R^2 = 0.78$, slope $= -0.000{,}86\ \mu\text{m}^{-1}$, $p < 0.0001$) and humeri ($R^2 = 0.89$, slope $= -0.000{,}79\ \mu\text{m}^{-1}$, $p < 0.0001$) (Fig. 5). These relationships demonstrate that an increase in tissue strain magnitude exacerbates the spatial extent of cell death on the articular surface under sustained subimpact loading conditions. Note that the y-intercepts of the fitted curves indicate the critical tissue strain $\left(E_z^{\text{critical}}\right)$ leading to in situ chondrocyte death. Interestingly, this threshold strain ($E_z^{\text{critical}} = -0.30$ for femurs and $E_z^{\text{critical}} = -0.29$ for humeri), as well as the slopes of the fitted curves ($-0.000{,}86\ \mu\text{m}^{-1}$ for femurs and $-0.000{,}79\ \mu\text{m}^{-1}$ for humeri), remained relatively consistent regardless of anatomical location.

Characterization of Poroelastic Creep Behavior. The poroelastic creep behavior of murine cartilage on the lateral femoral condyle and humerus was characterized using the established relationship between peak tissue strain (E_z) and radius of cell death ($r_{\text{cell death}}$) (Fig. 5) to convert $r_{\text{cell death}}$ versus loading duration curves (Fig. 4) to E_z versus loading duration curves (Fig. 6). The resulting creep responses demonstrated that compression of articular cartilage on both the femoral lateral condyles and the humeral heads surpassed the critical tissue strain ($E_z \sim -0.3\%$) within the first 10 s and gradually slowed until equilibrium was reached at approximately 1 min (Fig. 6).

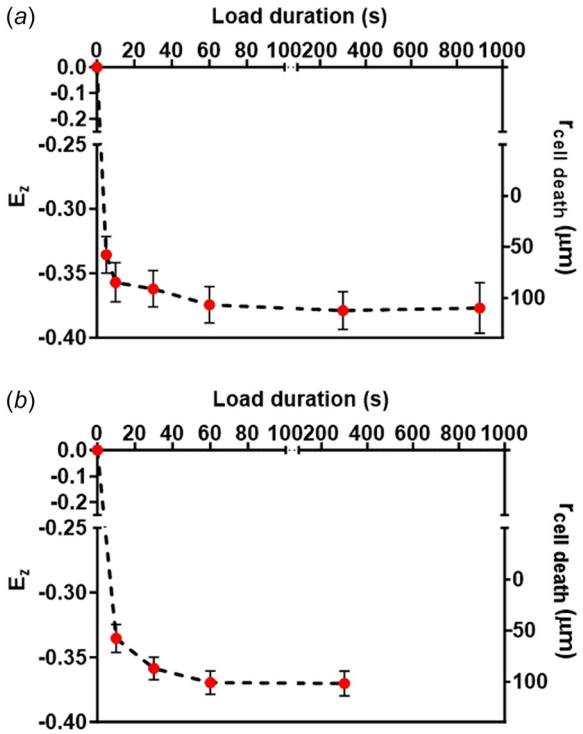

Fig. 6 Poroelastic creep curves depicting time-dependent strain and cell death induced by static loading. Temporal evolution of tissue strain (E_z, left axis) as determined from the radius of the area of cell death ($r_{\text{cell death}}$, right axis) in (*a*) femurs (lateral condyle) and (*b*) humeri after application of a 1 N static load for different durations. E_z was inferred from $r_{\text{cell death}}$ according to the previously established relationships (Fig. 5). The E_z versus loading duration curves resemble typical creep curves where E_z gradually increases in magnitude until equilibrium is reached. Data are mean ±SD, where SD is the standard deviation of E_z calculated using standard error propagation formulas.

Characterization of the Poroelastic Material Properties of Murine Articular Cartilage Using Inverse Finite Element Analysis. Inverse finite element analysis (iFEA) was used to determine murine cartilage poroelastic material properties based on specimen-specific geometric parameters and poroelastic creep curves generated as described earlier (Fig. 6). The Young's modulus (E) was found to be 12.2 MPa (Fig. S3 available in the Supplemental Materials on the ASME Digital Collection), while the hydraulic permeability (k) was found to be 0.86×10^{-16} m^4/N-s (Fig. 7).

Discussion

In this study, we tested intact cartilage-on-bone explants obtained from different anatomical locations using a previously developed microscope-mounted platform to isolate the effects of tissue deformation and strain on the viability of murine in situ chondrocytes. By applying prescribed subimpact load magnitudes with different durations, tissue strain was varied and the resulting spatial extent of cell death (i.e., $r_{\text{cell death}}$) was quantified. While $r_{\text{cell death}}$ depended on loading duration for a given load magnitude, we identified a consistent linear relationship between tissue strain and radius of cell death. Moreover, we showed that the relationship between tissue strain and $r_{\text{cell death}}$ can be used to convert $r_{\text{cell death}}$ versus loading duration curves to tissue strain versus loading duration curves (i.e., poroelastic creep curves). Finally, we showed that based on these creep curves (generated from measurements of mechanically induced cell death), poroelastic material properties can be inferred using an inverse finite element modeling procedure.

To investigate possible variations across joints, we established direct relationships between tissue strain (E_z) and the radius of the area of cell death $\left(r_{\text{cell death}}\right)$ on the articular surface for both femoral cartilage and humeral cartilage. For each anatomical location, these relationships revealed (1) the rate of change in cell death as a function of tissue strain (i.e., $r_{\text{cell death}}$ rate $= 1/$slope of the fitted E_z versus $r_{\text{cell death}}$ curve) and (2) the critical tissue strain (E_z^{critical}) above which the cells are killed. The similar values of $r_{\text{cell death}}$ rate and E_z^{critical} in femurs ($r_{\text{cell death}}$ rate $= -1.3 \times 10^3\ \mu$m, $E_z^{\text{critical}} = -0.30$) and humeri ($r_{\text{cell death}}$ rate $-1.2 \times 10^3\ \mu$m, $E_z^{\text{critical}} = -0.29$) suggest that murine in situ chondrocytes have the same sensitivity to subimpact mechanical loading regardless of anatomical location. Though not highly sensitive to anatomical location, the relationship between tissue strain and $r_{cell\ death}$ established in this study may depend on mouse strain, age, sex, or other variables. Nevertheless, once established, our data suggest that this relationship can be used to compute poroelastic material properties in murine cartilage based solely on cell death areas quantified from standard fluorescence micrographs.

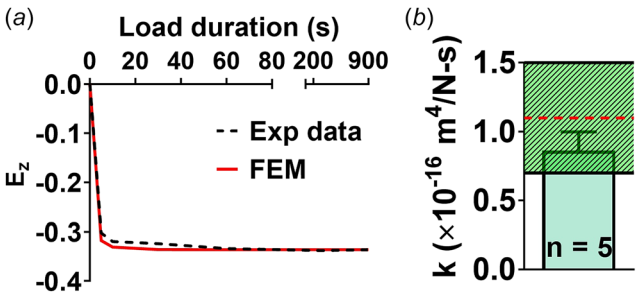

Fig. 7 Poroelastic/biphasic properties of AC determined via inverse finite element analysis. (*a*) Experimentally determined poroelastic creep curve (dashed line) and curve fit determined from inverse finite element analysis (solid line). (*b*) Hydraulic permeability (k) determined using iFEA. Data are mean ± SD. The dashed line and shaded area in (*b*) represents values (mean ± SD) obtained from literature [14].

According to our data, E_z^{critical} has a value of approximately −0.3 in articular cartilage under static loading. This finding is consistent with studies reporting that a nominal strain of −0.1 (leading to a superficial zone strain of −0.3) was required to kill chondrocytes in statically loaded of bovine cartilage explants [17]. Notably, compressive strains as high as 39% have been measured in vivo in static loading scenarios including standing on a single leg for several minutes [22]. Thus, our findings suggest that some static physiological activities may induce cell death in joints.

Using the approach developed in this study, the hydraulic permeability (k) of murine cartilage was found to be 0.86×10^{-16} m^4/N-s, consistent with the value reported in the literature based on micro-indentation tests ($k = 1.1 \pm 0.4 \times 10^{-16}$ m^4/N-s) [14]. The solid matrix Young's modulus (E) is murine cartilage was found to be 12.2 MPa—similar to values reported in previous studies from our lab and others [20,23], but higher than values reported in other published work [13,14]. Because our inverse finite element modeling procedure accounted for the geometry of the tissue and the presence of the rigid bone and glass slide, the large magnitude E in our study is unlikely to be a substrate effect. Instead, our measurement of E may be higher than some previous studies because our mechanical tests induced high compressive strains in the tissue (>30%, compared with < 5% in standard mechanical testing protocols), and cartilage is a highly nonlinear material with a solid matrix Young's modulus that increases with strain [24].

It is interesting to consider why $r_{\text{cell death}}$ grows over time under constant loading conditions, and what the underlying cause of the close relationship between $r_{\text{cell death}}$ and tissue strain (E_z) may be. In our experimental platform, a flat rigid surface (the glass slide) imparts a constant, static load on cartilage with a curved surface. In this incongruent geometry, as fluid squeezes from the biphasic/poroelastic tissue, two important phenomena occur: (1) the compressive strain in the tissue grows due to poroelastic creep; and (2) the contact area increases over time, reducing the contact pressure from the glass and stress within the cartilage. Thus, under these specific conditions, load is constant over time and stress diminishes over time. However, strain magnitude *increases* over time, similar to cell death area (Fig. 6). Collectively, these findings suggest that chondrocyte death may be triggered by tissue strain, but not by tissue load and stress. However, it is also possible that cell death area increases over time not because tissue strain magnitude is elevated, but rather because time-dependent growth of the contact area exposes an increasingly large region of cells to contact-induced stress above a critical level (despite an overall reduction of tissue stress). In this scenario, the close relationship between tissue strain and cell death area would not be causal, but would instead simply reflect that both cell death area and strain are separately correlated with contact area.

There are several limitations that must be considered in this study. First, cell death was quantified 5 min after the applied subimpact loading was removed, and thus only short-term cell death was analyzed. However, it is conceivable that cell death area could evolve over time due to repair of damaged/permeabilized membranes [25] or other slow processes, rendering cell death area measurements less reliable. Nevertheless, previous characterization of our in vitro murine model has demonstrated that the area of dead cells reduced by only ~5% within 3 h after removal of the injurious subimpact loads [19], suggesting that our cell death area measurements predominantly identify cells killed immediately by extreme loading conditions. Second, cell death was induced by the application of extreme subimpact loads (0.5 N and 1 N). These loads brought about compressive strains above 40% and local compressive stresses exceeding 16 MPa (according to FE simulations), which are higher than physiological strains and stresses reported in literature [22]. However, because extreme loads were applied, large, quantifiable areas of dead cells were produced, and the resultant wide range in the parameter $r_{\text{cell death}}$ was exploited to establish a relationship between $r_{\text{cell death}}$ and tissue strain (Fig. 4). Third, it is possible that storing specimens in −20 °C changes ECM mechanical properties, leading to overestimation of the peak tissue deformations. However, specimens from all experimental groups were frozen, and we do not anticipate that consistent tissue alterations caused by the freeze-thaw process affect the linear relationship between cell injury and tissue deformation. Fourth, in this study, we were only able to quantify cell death after the applied load was removed from the tested explants (Fig. S4 available in the Supplemental Materials on the ASME Digital Collection). Thus, we were unable to perform real-time visualization of cell death during poroelastic creep, presumably since the calcein dye—the indicator of viable cells—was "trapped" in the compressed tissue and could not leave damaged cells and diffuse through the compressed ECM (see Supplementary Materials). Consequently, we could not visualize temporally varying cell injury/death in real-time using a single specimen and therefore could not conduct a longitudinal study that would have significantly reduced the number of specimens required to establish poroelastic creep curves. Fifth, we used cyanoacrylate glue to stabilize humeral specimens prior to testing, and it is conceivable that cells were affected by the presence of glue. However, the finding that humeral specimens and femoral specimens exhibited similar trends suggested that the influence of glue on the acquired data was likely negligible. Sixth, since bone and cartilage size and morphology vary by sex, only female mice were used in this study to ensure consistent specimen size and cartilage geometry. While we expect E_z and $r_{\text{cell death}}$ to also strongly correlate in male mice, the specific quantitative relationship between these parameters may be sex-dependent. Thus, the sex-dependence of this quantitative relationship will be interrogated in future work. Seventh, there are gaps in the correlation plots used to determine the relationship between E_z and $r_{\text{cell death}}$ (Fig. 5), and it is conceivable that the absence of data in these regions could bias the linear fits. Thus, there is a need to fill these gaps in future studies. Nevertheless, we expect the data within these regions to follow trends consistent with the linear fit determined based on behavior at higher and lower levels of strain. Finally, while *intact* cartilage-on-bone explants faithfully reproduce the native mechanical and structural environment of in situ articular chondrocytes, some physiological external conditions (e.g., temperature and oxygen levels) were not maintained in this study. Nevertheless, all experiments were conducted under a consistent environment, allowing for fair comparisons between the experimental groups.

In conclusion, using an in vitro murine cartilage-on-bone explant model, we established a linear relationship between tissue strain and death of in situ chondrocytes in two different anatomical locations. We also demonstrated the key role poroelastic creep plays in mediating cell survival in intact cartilage subjected to sub-impact loading from an incongruent surface. In particular, we showed that poroelastic creep provides a time window (causes a delay) before cartilage surpasses critical tissue strain leading to cell death. Hence, prolonged static loading in incongruent joints may be associated with increased susceptibility to cell injury. Finally, we demonstrated that measurements of cell death overtime on the surface of cartilage exposed to constant loading conditions can be used—in combination with our established relationships between tissue strain and cell death area—to assess murine cartilage poroelastic material properties. In future studies, this approach can be applied in transgenic mouse models to delineate how specific genes modulate the macroscale poroelastic mechanical response of cartilage.

Acknowledgment

The authors thank Wenqi Di, Alex McMullen, Aldo Tecse, and Brian Wise for assistance with inter-rater reliability analysis.

Funding Data

- NSF CMMI (Award ID: 2217494; Funder ID: 10.13039/100000147).
- NIH (Award ID: R01 AR070765; Funder ID: 10.13039/100000069).

Data Availability Statement

The datasets generated and supporting the findings of this article are obtainable from the corresponding author upon reasonable request.

References

[1] Sophia Fox, A. J., Bedi, A., and Rodeo, S. A., 2009, "The Basic Science of Articular Cartilage: Structure, Composition, and Function," Sports Health, **1**(6), pp. 461–468.

[2] Buckwalter, J. A., and Mankin, H. J., 1998, "Articular Cartilage: Tissue Design and Chondrocyte-Matrix Interactions," Instr. Course Lect., **47**, pp. 477–486.

[3] Mow, V. C., Kuei, S. C., Lai, W. M., and Armstrong, C. G., 1980, "Biphasic Creep and Stress Relaxation of Articular Cartilage in Compression? Theory and Experiments," ASME J. Biomech. Eng., **102**(1), pp. 73–84.

[4] Basalo, I. M., Mauck, R. L., Kelly, T. A., Nicoll, S. B., Chen, F. H., Hung, C. T., and Ateshian, G. A., 2004, "Cartilage Interstitial Fluid Load Support in Unconfined Compression Following Enzymatic Digestion," ASME J. Biomech. Eng., **126**(6), pp. 779–786.

[5] Thambyah, A., Heeswijk, V. V., Donkelaar, C. C. V., and Broom, N. D., 2015, "A Microstructural Study of Load Distribution in Cartilage: A Comparison of Stress Relaxation Versus Creep Loading," Adv. Mater. Sci. Eng., **2015**, pp. 1–11.

[6] Malekipour, F., Whitton, C., Oetomo, D., and Lee, P. V., 2013, "Shock Absorbing Ability of Articular Cartilage and Subchondral Bone Under Impact Compression," J. Mech. Behav. Biomed. Mater., **26**, pp. 127–135.

[7] Malekipour, F., Lee., and P. V. S., Shaktivesh, 2019, "Shock Absorbing Ability in Healthy and Damaged Cartilage-Bone Under High-Rate Compression," J. Mech. Behav. Biomed. Mater., **90**, pp. 388–394.

[8] Gleghorn, J. P., and Bonassar, L. J., 2008, "Lubrication Mode Analysis of Articular Cartilage Using Stribeck Surfaces," J. Biomech., **41**(9), pp. 1910–1918.

[9] Burris, D. L., Ramsey, L., Graham, B. T., Price, C., and Moore, A. C., 2019, "How Sliding and Hydrodynamics Contribute to Articular Cartilage Fluid and Lubrication Recovery," Tribol. Lett., **67**(2), p. 46.

[10] Ateshian, G. A., 2009, "The Role of Interstitial Fluid Pressurization in Articular Cartilage Lubrication," J. Biomech., **42**(9), pp. 1163–1176.

[11] McCutchen, C. W., 1962, "The Frictional Properties of Animal Joints," Wear, **5** (1), pp. 1–17.

[12] Chery, D. R., Han, B., Li, Q., Zhou, Y., Heo, S. J., Kwok, B., Chandrasekaran, P., Wang, C., Qin, L., Lu, X. L., et al., 2020, "Early Changes in Cartilage Pericellular Matrix Micromechanobiology Portend the Onset of Post-Traumatic Osteoarthritis," Acta Biomater., **111**, pp. 267–278.

[13] Doyran, B., Tong, W., Li, Q., Jia, H., Zhang, X., Chen, C., Enomoto-Iwamoto, M., Lu, X. L., Qin, L., and Han, L., 2017, "Nanoindentation Modulus of Murine Cartilage: A Sensitive Indicator of the Initiation and Progression of Post-Traumatic Osteoarthritis," Osteoarthritis Cartilage, **25**(1), pp. 108–117.

[14] Cao, L., Youn, I., Guilak, F., and Setton, L. A., 2006, "Compressive Properties of Mouse Articular Cartilage Determined in a Novel Micro-Indentation Test Method and Biphasic Finite Element Model," ASME J. Biomech. Eng., **128**(5), pp. 766–771.

[15] Chiravarambath, S., Simha, N. K., Namani, R., and Lewis, J. L., 2009, "Poroviscoelastic Cartilage Properties in the Mouse From Indentation," ASME J. Biomech. Eng., **131**(1), p. 011004.

[16] Nia, H. T., Gauci, S. J., Azadi, M., Hung, H. H., Frank, E., Fosang, A. J., Ortiz, C., and Grodzinsky, A. J., 2015, "High-Bandwidth AFM-Based Rheology is a Sensitive Indicator of Early Cartilage Aggrecan Degradation Relevant to Mouse Models of Osteoarthritis," J. Biomech., **48**(1), pp. 162–165.

[17] Torzilli, P. A., Deng, X. H., and Ramcharan, M., 2006, "Effect of Compressive Strain on Cell Viability in Statically Loaded Articular Cartilage," Biomech. Model Mechanobiol., **5**(2–3), pp. 123–132.

[18] Kotelsky, A., Carrier, J. S., Aggouras, A., Richards, M. S., and Buckley, M. R., 2020, "Evidence That Reduction in Volume Protects in Situ Articular Chondrocytes From Mechanical Impact," Connect. Tissue Res., **61**(3–4), pp. 360–374.

[19] Kotelsky, A., Carrier, J. S., and Buckley, M. R., 2019, "Real-Time Visualization and Analysis of Chondrocyte Injury Due to Mechanical Loading in Fully Intact Murine Cartilage Explants," J. Visualized Exp., **143**, p. e58487.

[20] Kotelsky, A., Woo, C. W., Delgadillo, L. F., Richards, M. S., and Buckley, M. R., 2018, "An Alternative Method to Characterize the Quasi-Static, Nonlinear Material Properties of Murine Articular Cartilage," ASME J. Biomech. Eng., **140** (1), p. 011007.

[21] Galbraith, W., 1955, "The Optical Measurement of Depth," Q. J. Microsc. Sci., **S3-96**(35), pp. 285–288.

[22] Halonen, K. S., Mononen, M. E., Jurvelin, J. S., Töyräs, J., Salo, J., and Korhonen, R. K., 2014, "Deformation of Articular Cartilage During Static Loading of a Knee Joint–Experimental and Finite Element Analysis," J. Biomech., **47**(10), pp. 2467–2474.

[23] Kabir, W., Di Bella, C., Choong, P. F. M., and O'Connell, C. D., 2021, "Assessment of Native Human Articular Cartilage: A Biomechanical Protocol," Cartilage, **13**(2_suppl), pp. 427 s–437 s.

[24] Fortin, M., Soulhat, J., Shirazi-Adl, A., Hunziker, E. B., and Buschmann, M. D., 2000, "Unconfined Compression of Articular Cartilage: Nonlinear Behavior and Comparison With a Fibril-Reinforced Biphasic Model," ASME J. Biomech. Eng., **122**(2), pp. 189–195.

[25] McNeil, P. L., and Kirchhausen, T., 2005, "An Emergency Response Team for Membrane Repair," Nat. Rev. Mol. Cell Biol., **6**(6), pp. 499–505.